Electronic Structure and Carrier Mobility in Graphdiyne Sheet and Nanoribbons: Theoretical Predictions

Mengqiu Long,[†] Ling Tang,[†] Dong Wang,[†] Yuliang Li,[‡] and Zhigang Shuai*[,†,‡]

[†]Key Laboratory of Organic OptoElectronics and Molecular Engineering, Department of Chemistry, Tsinghua University, Beijing 100084, P. R. China, and [‡]Key Laboratory of Organic Solids, Beijing National Laboratory for Molecular Sciences (BNLMS), Institute of Chemistry, Chinese Academy of Sciences, Beijing 100190, P. R. China

ABSTRACT Using density functional theory coupled with Boltzmann transport equation with relaxation time approximation, we investigate the electronic structure and predict the charge mobility for a new carbon allotrope, the graphdiyne for both the sheet and nanoribbons. It is shown that the graphdiyne sheet is a semiconductor with a band gap of 0.46 eV. The calculated in-plane intrinsic electron mobility can reach the order of 10^5 $cm^2/(V\ s)$ at room temperature, while the hole mobility is about an order of magnitude lower.

KEYWORDS: graphdiyne sheet · nanoribbons · mobility · density functional theory · Boltzmann transport

Over the past twenty years, tremendous efforts have been devoted to searching new carbon allotropes, and many types of carbon forms such as fullerene,[1] carbon nanotube,[2] and graphene,[3] have been added to the family of carbon. One new carbon form, graphyne, has been first theoretically proposed,[4] which consists of planar molecular sheets containing only sp and sp^2 carbon atoms. Among various graphyne structures, graphdiyne has been targeted by Haley, Brand, and Pak[5] in 1997 and since then great efforts have been devoted to the synthesis of monomeric and oligomeric substructures toward constructing graphdiyne.[6−8] Only until very recently, large area ($\sim$ 3.6 cm^2) of graphdiyne film has been successfully prepared *via* cross-linking reaction using hexaethynylbenzene on top of copper surface,[9] which has been demonstrated to exhibit good semiconducting properties. Nevertheless, single sheet of graphdiyne is still not available, which is a highly challenging task.

Graphdiyne is one of the most "synthetically approachable" allotropes[10] containing two acetylenic (diacetylenic) linkages between carbon hexagons. Graphdiyne has been predicted to exhibit fascinating properties including high third-order nonlinear optical susceptibility, high fluorescence efficiency, extreme hardness, high thermal resistance, conductivity or superconductivity, and through-sheet transport of ions.[4,10−15] Graphdiyne is also predicted to be the most stable carbon network containing diacetylenic linkages.[16−19] In this work, we investigate the electronic structure and the charge transport properties through first principles calculations, especially for predicting the charge mobility for the graphdiyne sheet and for its various nanoribbons.

Charge transport properties in these new carbon allotrope materials have become the center of interests, because of their unique physical, chemical, and structural properties and potential for use in next generation electronic devices.[20−22] Carrier mobility is the central issue for microelectronic semiconducting materials. The single-wall carbon nanotubes and graphene nanoriboons have been demonstrated to possess charge mobility as high as 7.9×10^4 $cm^2/(V\ s)$[23] and $2-25 \times 10^4$ $cm^2/(V\ s)$[24−30] at room temperature, respectively. As a new type of carbon allotrope material, both theoretical and experimental studies have indicated that graphdiyne is semiconductor.[9,12] The potential application of graphdiyne in the future nanoelectronics is of great interest. It is the primary motivation of this work to predict the intrinsic carrier mobility for an ultrapure single layered graphdiyne as well as its nanoribbons.

RESULTS AND DISCUSSION

The graphdiyne sheet structure is shown in Figure 1, where the unit cell is drawn with dashed line. The VASP optimized lattice constant is found to be $a_0 = 9.48$ Å, in good agreement with the previous value of 9.44 Å calculated by Narita *et al.*[13] with the local density approximation. The energy band

* Address correspondence to zgshuai@tsinghua.edu.cn.

Received for review September 21, 2010 and accepted March 21, 2011.

Published online March 28, 2011
10.1021/nn102472s

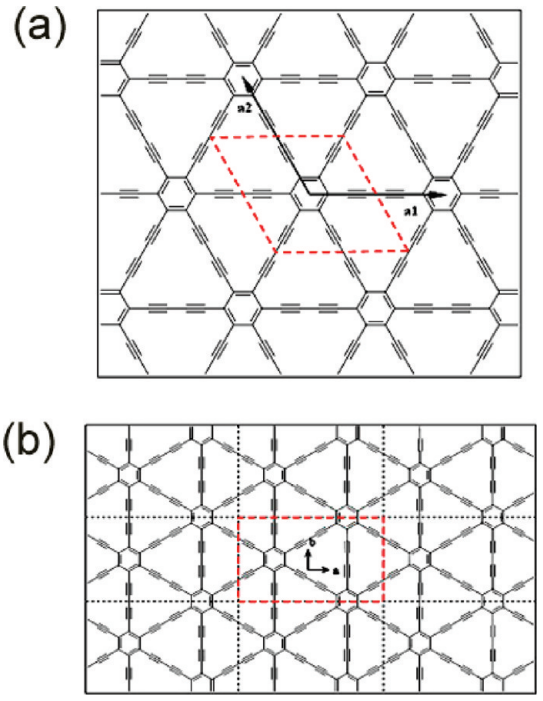

Figure 1. Schematic representation of a single graphdiyne sheet. The lattice vectors are given by $\vec{a}_1 = a_0\vec{x}$ and $\vec{a}_2 = a_0(-\vec{x}2/ + (3^{1/2}\vec{y})/2)$. The rhombus drawn with dashed line represents the primitive cell. The super cell used for transport calculations (dashed rectangle) is also shown, which contains 36 carbon atoms.

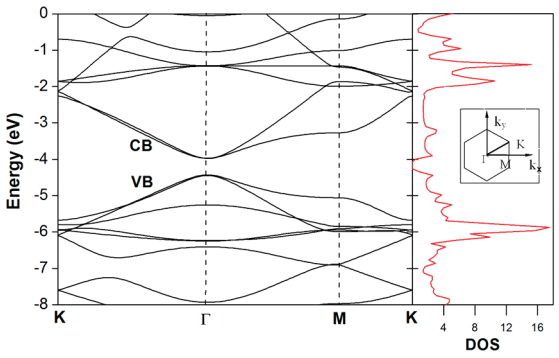

Figure 2. Band structure and density of states for single graphdiyne sheet obtained from DFT calculations. The Brillouin zone is also shown.

structure calculated for a single graphdiyne sheet is shown in Figure 2. The band dispersion arises mostly from the overlap of the carbon $2p_z$ orbitals. It is seen that the graphdiyne is a semiconductor with a band gap of 0.46 eV at the Γ-point. It should be noted that the band gap of semiconducting materials is underestimated by the density functional theory (DFT) calculations that do not include the self-energy from many-electron interactions. Since our deformation potential (DP) method only considered the shifts of valence band (VB) and conduction band (CB), the actual value of band gap does not affect appreciably the transport property calculations, but the curvature of the bands, which may not be correctly characterized by DFT, can affect the effective mass and mobility.

In the charge transport calculation, we build a supercell along two vertical directions **a** and **b** for graphdiyne sheet which allows for more intuitive explanation for transport property, as shown in Figure 1. There are 36 atoms in this rectangular super cell. Lattice constants are a_0 = 16.42 Å and b_0 = 9.48 Å for the supercell at equilibrium geometry. To calculate the deformation potential constant E_1 and the stretching modulus C^β (here we use β for generic index), we dilate the super cell of graphidyne uniformly along the direction **a** or **b**, and calculate the band structures at different degrees of dilation in the range of ±0.5%. By fitting the curve of the total energy E of the super cell with respect to dilation $\Delta l/l_0$ as $(E - E_0)/S_0 = C^\beta(\Delta l/l_0)^2/2$, we can evaluate the elastic constant of the sheet along the transport direction β. Here S_0 and E_0 are area and total energy of the super cell at the optimized structure. Δl is the deformation of lattice constant along the direction β and l_0 is its value at equilibrium geometry, a_0 or b_0. The DP constant is defined as $E_1 = \Delta E/(\Delta l/l_0)$, where ΔE is energy shift of the band edge position with respect to the lattice dilation $\Delta l/l_0$ along the direction β of the external field. For low carrier concentration, the charges are near the band edge. So we take the energy shift at the upper edge of the valence band for hole and at the lower edge of the conduction band for electron. As shown in Figure 2, both the conduction band and the valence band of the graphdiyne-sheet are quasi-degenerate along the Γ-K direction. This quasi-degeneracy raise the interband-scattering probability, which is not accounted for by the deformation potential theory presented here. However, we can tell from eqs (A31) and (A32) of Bardeen and Shockley's work[31] that the interband transition matrix element at small momentum **P** vanishes to the zero-th order approximation since the wave functions of the degenerate bands are orthogonal to each other. So the interband-scattering probability is a small quantity in camparison with the intraband-scattering probability and neglection of it should have minor impact on the relaxation times. If not considering interband-scattering, the degenaracy will only increase the density of states, but not alter the mobilities (see eq 2 below in METHODS).

In Figure 3a, we present the calculated band edge positions of the VB and CB at the Γ-point as a function of the dilation, along the direction **a**. Around the equilibrium structure, the band edge position changes linearly with the lattice deformation, with the slope being the DP constant E_1. In Figure 3b, we present the total energy of super cell for graphdiyne as a function of lattice dilation along both **a** and **b** directions. With parabola fittings, the corresponding stretching modulus can be calculated.

Table 1 shows all the calculated DP constants, the stretching modulus, the carrier mobilities and the

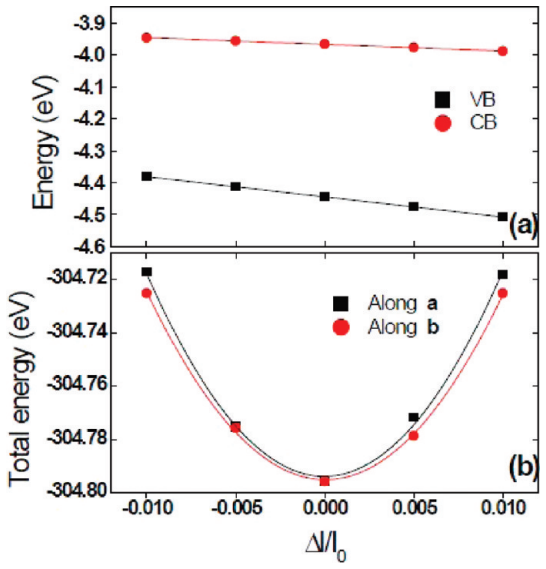

Figure 3. (a) The band edge positions of VB and CB with respect to the lattice dilation $\Delta l/l_0$ along the a direction for the graphdiyne sheet. Solid lines represent the linear fit, which defines DP constant. (b) The total energy of a unit cell as a function of lattice deformation along the a and b directions. Solid lines are the parabola fittings, which give elastic constant.

TABLE 1. Deformation Potential E_1, Elastic Constant C, Carrier Mobility μ, and the Averaged Value of Scattering Relaxation Time τ at 300 K for Electrons and Holes in a Single Graphdiyne Sheet

carrier type	E_1 (eV)	C (J/m^2)	μ (10^{4}cm^2/(V s))	τ (ps)
e[a]	2.09	158.57	20.81	19.11
h[a]	6.30	158.57	1.97	1.94
e[b]	2.19	144.90	17.22	15.87
h[b]	6.11	144.90	1.91	1.88

[a] The stretching direction **a**. [b] The stretching direction **b**.

relaxation times for both hole (valence band) and electron (conduction band). The mobility and relaxation time are calculated according to eq 2 and eq 3 given in METHODS. We can find that the in-plane mobilities along direction **a** and **b** are close to each other in Table 1. It is found that the intrinsic electron mobility can reach 2×10^5 cm^2/(V s), while the hole mobility is close to 2×10^4 cm^2/(V s), which is an order of magnitude lower than the mobility of electron at the room temperature (RT). The acoustic phonon scattering relaxation times are calculated to be 2 and 20 ps for hole and electron, respectively, which are close to the value for graphene.[32,33] It is clearly seen from Table 1 that the deformation potential E_1 value for hole is three times as large as that for electron. This results in a difference of ~1 order of magnitude in the mobilities of electron and hole by virtue of eq 2. The DP constant is a characterization of the coupling strength of the electron or hole to the acoustic phonon. The fact that the hole is more strongly scattered by the acoustic phonon than the electron can be understood by examining the frontier molecular orbitals responsible for transport. The band shift upon stretching comes from the site energy change, so if the orbital has more nodes in the direction of dilation, its site energy will be more prone to change upon dilation. The Γ-point highest occupied molecular orbital (HOMO) and lowest unoccupied molecular orbital (LUMO) are shown in Figure 4. Since the HOMO and LUMO are both degenerate, a pair of orbitals for either of them are plotted in Figure 4. The HOMO exhibits antibonding character between carbon hexagons and diacetylenic linkages therefore it has more nodes in either direction **a** or direction **b**, whereas the LUMO exhibits bonding character between carbon hexagons and diacetylenic linkages so it has less nodes in the directions of dilation, which makes the hole more prone to acoustic phonon scattering than the electron. The degenerate HOMO and LUMO at Γ−point and corresponding energies before and after dilation have been provided as Supporting Information.

We next examined the graphdiyne nanoribbons (GDNRs), which are important in nanoelectronic engineering. There are two major ways to cut the sheet into ribbons, as shown in Figure 5a, namely, cutting the graphdiyne along the direction of the nearest neighbor carbon hexagons (**A** → **B**) resulting in divan-like edged GDNR (DGDNR, Figure 5a-I), or cutting the sheet along the direction of the next nearest neighbor carbon hexagons (**A** → **C**), resulting in a zigzag-like edge of GDNR (ZGDNR, Figure 5a-II). Furthermore, there are two different ZGDNRs: the uniform width (Figure 5a-II) and nonuniform width (Figure 5a-III) by cutting at different sites.

In the present work, we examine five types of nanoribbons, as shown in Figure 5b−f. D1 and D2 are DGDNRs with two and three carbon hexagons in edge, respectively. Z1 and Z2 are ZGDNR with two and three carbon hexagons in edge, respectively, and Z3 is ZGDNR with two carbon hexagons at the narrow site and three hexagons at the broad site in edge. In order to avoid dangling bond at edge, the carbon atoms are passivated with hydrogen atoms at both the divan and zigzag edges for all the five types of GDRNs. The widths of the GDNRs are found to be 12.5 Å, 20.7 Å, 19.2 Å and 28.6 Å for D1, D2, Z1 and Z2, respectively, and the narrow width of Z3 is 19.2 Å and the broad width is 28.6 Å.

With the same theoretical methods employed for single graphdiyne sheet, we also calculated band structures and carrier mobilities of the five GDNRs. The band structures for GDNRs obtained from DFT calculations are shown in Figure 6. From the band structures, all GDNRs are predicted to be semiconductor, in which the smallest band gap (D2) has a value of

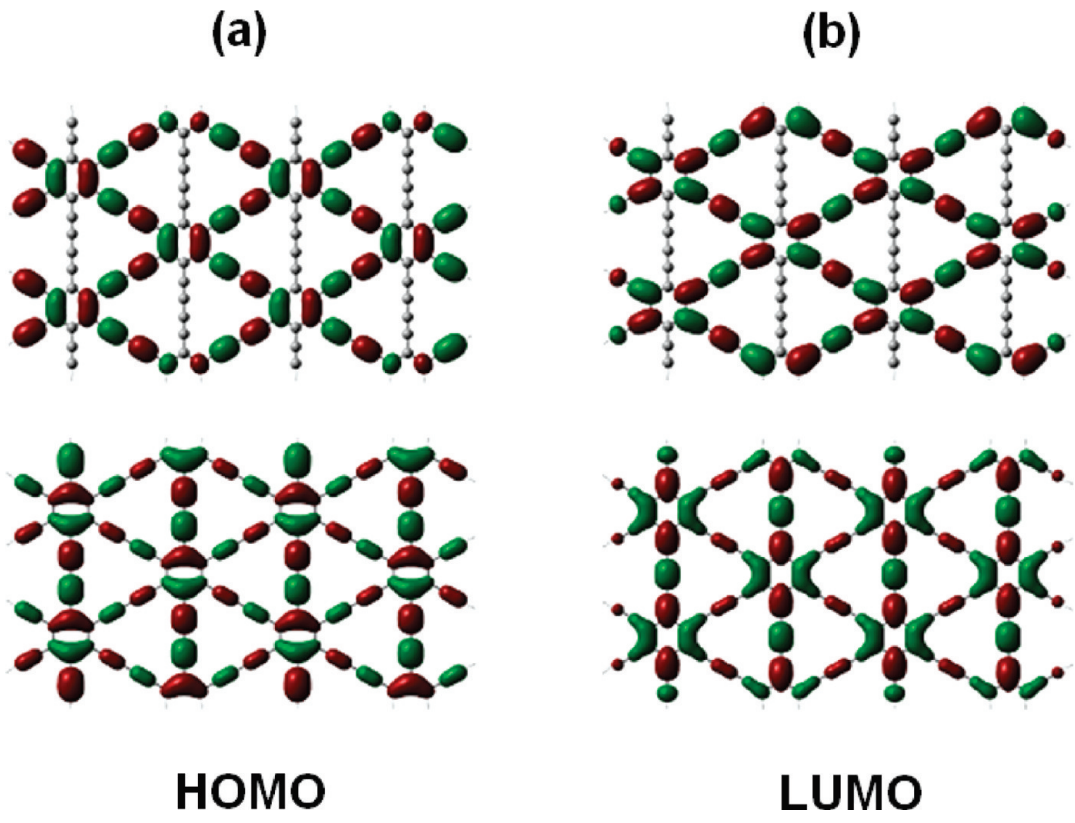

Figure 4. Γ-point degenerate HOMO and LUMO for the graphdiyne sheet. Note the number of nodes for the HOMO is more than that for the LUMO in either direction, which leads to the hole more strongly scattered by the acoustic phonon than the electron.

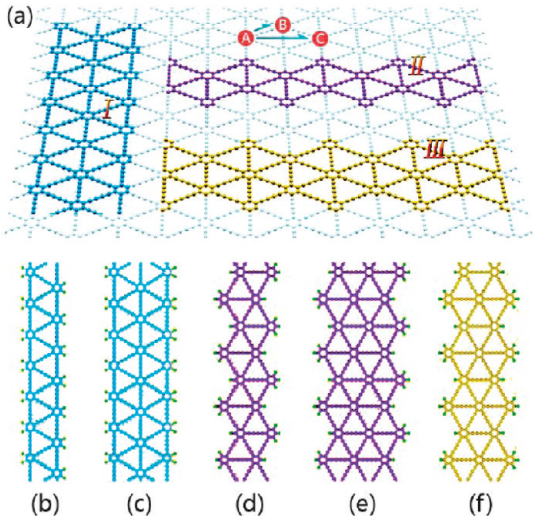

Figure 5. (a) Schematic representation of three graphdiyne nanoribbons building blocks: (I) a divan-like edged GDNR, (II) a zigzag-like edged GDNR with uniform width, (III) a zigzag GDNR with alternating width. Structures b and c are divan GDNRs with two and three carbon hexagons in width, respectively. Structures d and e are zigzag GDNRs with two and three carbon hexagons in width, respectively. Structure f is zigzag GDNR with two carbon hexagons at the narrow site and three at the broad site in width.

~0.8 eV at the Γ-point, which can be a useful feature for employing the GDNRs as semiconducting channels in FETs.

The calculated DP values for GDNRs are presented in Figure 7a. It is noted that E_1 for the hole is larger than E_1 for the electron for all GDNRs, same as that found for the graphdiyne sheet. The same antibonding feature between carbon hexagons and diacetylenic linkages has been found for the HOMO, whereas the bonding feature between hexagons and diacetylenic linkages is found for the LUMO (Figure 8). So the coupling strength between the hole and the acoustic phonon is larger than that between the electron and the acoustic phonon. The RT carrier mobilities for GDNRs calculated from eq 1 are also plotted in Figure 7b. It is found that the intrinsic electron mobility can reach the order of 10^4 $cm^2/(V\ s)$, and significantly larger than that of the hole mobility. It is also clearly seen that the charge mobility increases with the width within the same class GDNRs, and the DGDNRs is more favorable than the ZGDNRs for the electron transport. It is noted that for two-dimensional graphdiyne sheet charge carrier transport is almost isotropic. In contrast for one-dimensional GDNRs, electronic confinement becomes dominant, so upon cutting the sheet into ribbons, transport behaviors vary significantly and depend strongly on the direction of cutting. Figure 8 shows that the LUMO for D1 is much more delocalized in the direction of ribbon axis than that for Z1, so that the electron mobility for the former is much larger than the latter.

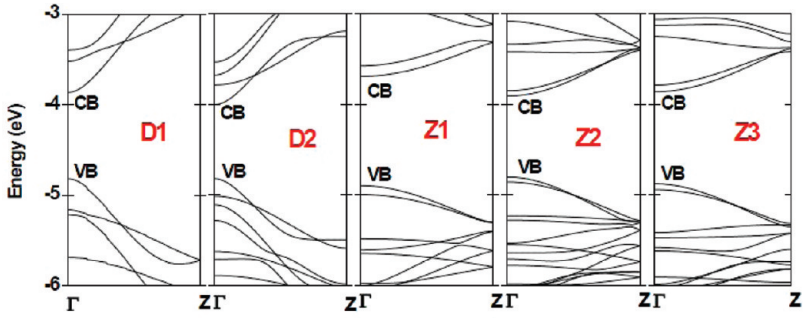

Figure 6. Band structures of GDNRs including two divan-like edged GDNRs D1 and D2 and three zigzag-like edged GDNRs Z1, Z2, and Z3. The structures of these GDNRs are given in Figure 5b–f, with D2 wider in edge than D1 and Z2 wider than Z1. Z3 has an edge width alternating between Z1 and Z2.

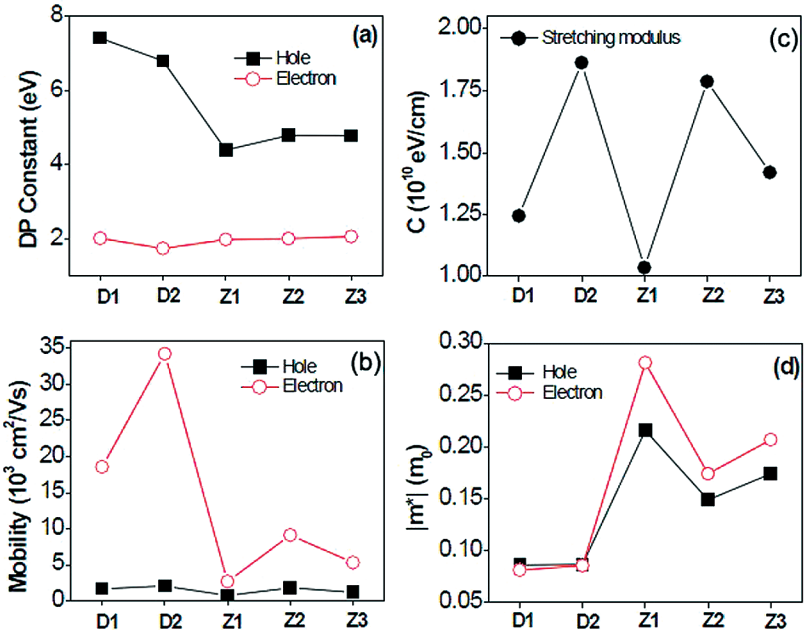

Figure 7. (a) DP constants for holes and electrons. (b) charge mobility for holes μ_h and electrons μ_e. (c) stretching modulus *C*. (d) effective masses $|m_h^*|$ and $|m_e^*|$ for five GDNRs D1, D2, Z1, Z2, and Z3.

To better understand the charge transport behaviors of GDNRS, we also employed the effective mass approximation in combination with the DP theory. With the parabolic approximation for the band structure of GDNRs, we can write the dispersion relation for band *i* as $\varepsilon_i(k) = \varepsilon_{0i} + (\hbar^2/2m_i^*)(k - k_0)^2$, where ε_{0i} is the band minimum, m_i^* is m_h^*, the effective mass of hole, or m_e^*, the effective mass of electron, and k_0 is the value of wave vector at the top of VB or at the bottom of CB. The use of an analytical parabolic expression, for the edge of the VB and CB facilitates the calculation of the charge injection effects. In this sense, the effective mass is simply associated with the parabolic fitting of the dispersion relation as $m^* = \hbar^2[\partial^2\varepsilon(k)/\partial k^2]^{-1}$. Under the effective mass approximation and the electron-acoustic phonon scattering mechanism, Bardeen and Shockley[31] derived an analytical expression for the intrinsic carrier mobility, and Beleznay *et al.*[34] have reformulated for one-dimensional case, which was employed to study the charge transport in carbon nanotubes[35] and graphene nanoribbons:[32]

$$\mu = \frac{e\bar{\tau}}{|m^*|} = \frac{e\hbar^2 C}{(2\pi k_B T)^{1/2}|m^*|^{3/2}E_1^{\,2}} \qquad (1)$$

where τ is the scattering relaxation time, $C = a_0(\partial^2 E/\partial a^2)|_{a=a_0}$ is the stretching modulus of one-dimensional system, a_0 is the lattice constant. The calculated stretching modulus for GDNRs are shown in Figure 7c. It is interesting to note that the stretching modulus slightly increases with the width in the same class of GDNRs (DGDRNs or ZGDNRs). And the stretching modulus of DGDNR is larger than that of ZGDNR with the same width. For instance, comparing D2 and Z1, their widths are close to each other, their stretching modulus differ by a factor of almost two. From the shape of the band structures shown in Figure 6, we can fit two curves the energy $\varepsilon(k)$ versus k points for

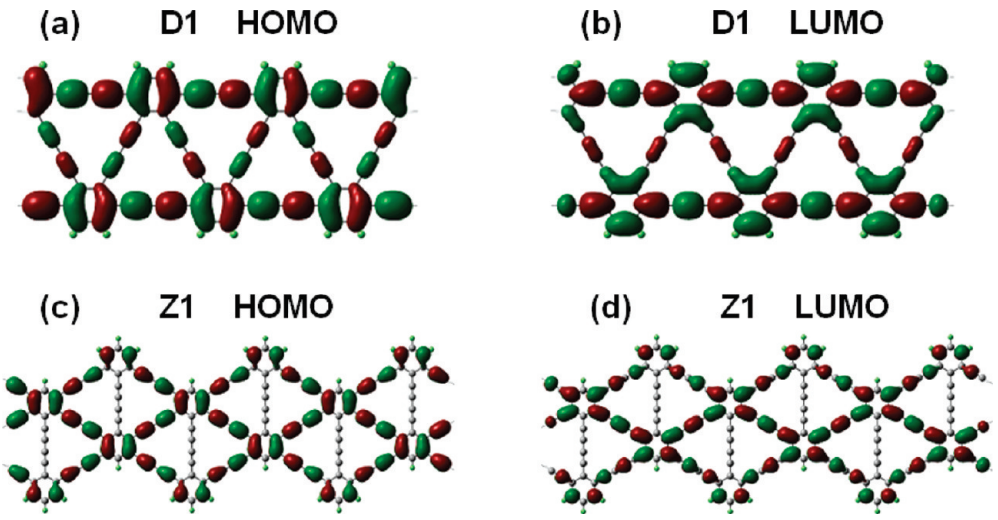

Figure 8. Γ-point HOMO and LUMO for GDNRs D1 and Z1. Note that for both D1 and Z1, the LUMO is more extended than the HOMO in the direction of cutting, which leads to larger electron mobility than the hole. Also, the LUMO for D1 exhibits much more delocalized character along the ribbon axis than that for Z1, which can qualitatively explain the fact that the electron mobility for D1 is larger than Z1.

TABLE 2. Calculated Band Gap, Effective Mass (m_h^* and m_e^*), DP Constants for VB and CB (E_v and E_c), Stretching Modulus C, and Carrier Mobility μ at 300 K for five GDNRs[a]

	D1	D2	Z1	Z2	Z3
band gap	0.954	0.817	1.205	0.895	1.015
$m_h^*(m_0)$	0.086	0.087	0.216	0.149	0.174
$m_e^*(m_0)$	0.081	0.086	0.281	0.174	0.207
E_v(eV)	7.406	6.790	4.386	4.786	4.776
E_e(eV)	2.006	1.730	1.972	2.000	2.054
$C(10^{10}$ eV/cm)	1.244	1.864	1.035	1.787	1.420
$\mu_h(10^3$ cm^2/(V s))	1.696	2.088	0.755	1.815	1.194
$\mu_e(10^3$ cm^2/(V s))	18.590	34.241	2.692	9.127	5.329
$\mu_h^*(10^3$ cm^2/(V s))	0.711	1.253	0.426	1.073	0.679
$\mu_e^*(10^3$ cm^2/(V s))	10.580	19.731	1.418	5.015	2.829

[a] μ_h and μ_e are calculated from eq 2, while μ_h^* and m_e^* are calculated from eq 1 under the effective mass approximation.

the top of VB and bottom of the CB near Γ-point, so we get the effective mass m_h^* and m_e^* for hole and electron, respectively as shown in Figure 7d. We find that the effective masses of DGNRs are smaller than those of ZGNRs, suggesting that DGNRs are better for charge carrier transport than ZGNRs.

We then calculated the charge mobility for GDNRs at RT based on eq 1. All the calculated results are shown in Table 2. We find that the results obtained from effective mass approximation are in good agreement with those from the Boltzmann transport theory. For instance, for D1, the electron mobility calculated from the Boltzmann method is 1.859×10^4 cm^2/(V s), compared well with 1.058×10^4 cm^2/(V s) of effective mass approximation.

In Table 2, we can find that the carrier mobility has manifested three characteristics for GDNRs: (i) the mobility increases slightly with the width of the same class GDNRs; (ii) the mobility of DGDNRs is larger than that of the ZGDNRs, especially for electrons, when the width of ribbons is similar, and (iii) the electron mobility is larger than that for hole in all GDNRs. From the details in Table 2, we found the stretching modulus C increases slightly with the width of the same class of GDNRs, which results in the behavior (i) mentioned above. For instance, D2 is wider than D1, so the stretching modulus of D2 is larger than that of D1, which causes the mobility of D2 larger than that of D1. For zigzag-type nanoribbons, the width of Z1, Z2, and Z3 is in the order of Z1 < Z3 < Z2, so is the magnitude of stretching modulus. In addition, the effective mass is in the opposite order, Z1 > Z3 > Z2. According to eq 1, the mobility is proportional to the stretching modulus C and inversely proportional to the effective mass $|m^*|^{3/2}$, so the mobility of zigzag-type nanoribbons increases with the width of the nanoribbons. Table 2 also shows that the effective masses of DGDNRs are about 0.08 m_0 (where m_0 is the free electron mass), and the electrons and holes possess almost the same mass, which is close to the result of graphdiyne sheet, 0.073 m_0 calculated by Narita *et al.*[13] While for ZGDNRs, the effective masses are significantly larger than those of DGDNRs, which are in the range of 0.15−0.28 m_0, with electrons being slightly larger than holes. This difference in effective masses finally leads to the electron mobilities of DGDNRs 1 order magnitude larger than those of ZGDNRs. The values of DP constants for electron and hole, which represent the scattering of a hole or electron from the acoustic phonon, are also shown in Table 2. It is found that E_1 for hole is larger than that for electron for each system, which is about three times as much as for DGDNRs and twice as that for ZGDNRs. Since carrier mobility is inversely proportional to the square of DP constant, we find that the electron mobility is approximately 1 order of magnitude larger than that of hole for each DGDNR, while for each

ZGDNR, the electron mobility is about four times larger than that of hole. As for the graphdiyne sheet, holes are more strongly scattered by the acoustic phonon than electrons in GDNRs, which can be understood by the bonding character of HOMO and LUMO responsible for transport.

CONCLUSIONS

In conclusion, we have calculated the intrinsic charge carrier mobility of the graphdiyne sheet and GDNRs scattered by the longitudinal acoustic phonon, using first-principles density functional theory and the Boltzmann transport equation with the relaxation time approximation. The numerical results indicate that the electron mobility can reach 2×10^5 cm^2/(V s) at room temperature for single graphdiyne sheet, while the hole mobility is an order of magnitude lower. The room temperature electron mobility of GDNRs can also reach 10^4 cm^2/(V s), and significantly larger than that of the hole mobility. We also found that the charge mobility increases with the width in GDNRs, and the divan-edged GDNRs have larger mobility than the zigzag edged GDNRs.

METHODS

Following the argument of Shockley and Bardeen,[31] the dominant scattering of a thermal electron or hole arises mostly from the acoustic phonons, since the electron coherence length is close to the acoustic phonon wavelength and much longer than the bond length. This is expected to be the case for graphdiyne sheet. Earlier, we have shown that in graphene nanoribbons, the acoustic phonon mechanism can well account for the charge transport behavior,[32] where a deformation potential theory was used to calculate the scattering relaxation time with the Boltzmann transport equation. Here, we expect the same acoustic phonon scattering mechanism could be appropriately applied because of the covalently bonded conjugated structure in graphdiyne.

In the present work, the electronic structures are calculated using first-principles density functional methods and the charge mobility is evaluated based on the Boltzmann transport equation within the DP theory for both single-layer graphdiynes and its nanoribbons. Geometry optimization and the band structure calculations were carried out using density-functional theory as implemented in Vienna *ab initio* simulation package (VASP)[36−39] with a projector-augmented-wave method.[40] The generalized gradient approximation of Perdew-Burke-Ernzerhof exchange correlation functional was used,[41] and the kinetic energy cutoff was chosen to be 500 eV. The optimizations using constrained unit-cell parameters are done until all the atomic forces are less than 0.01 eV/Å, and the convergence criterion of the total energy is 10^{-5} eV in the self-consistent field iteration. The supercell is large enough to ensure that the vacuum space is at least 20 Å.

Within the Boltzmann transport method, the carrier mobility μ in the relaxation time approximation can be expressed as[42,43]

$$\mu_\alpha^{e(h)} = \frac{e}{k_B T} \frac{\sum_{i\in CB(VB)} \int \tau_\alpha(i,\vec{k}) v_\alpha^2(i,\vec{k}) \exp\left[\mp \frac{\varepsilon_i(\vec{k})}{k_B T}\right] d\vec{k}}{\sum_{i\in CB(VB)} \int \exp\left[\mp \frac{\varepsilon_i(\vec{k})}{k_B T}\right] d\vec{k}} \quad (2)$$

where α denotes the direction of external field and the minus (plus) sign is for electron (hole). $\varepsilon_i(\vec{k})$ and $v_\alpha(i,\vec{k})$ are band energy and the α component of group velocity at $\vec{k}$ state of the ith band, respectively. The summation of band was carried out over VB for hole and CB for electron. Furthermore, the integral of $\vec{k}$ states is over the first Brillouin zone (BZ).

To obtain the mobility, there are three key quantities to be determined, namely, $\varepsilon_i(\vec{k})$, $v_\alpha(i,\vec{k})$ and $\tau_\alpha(i,\vec{k})$. In this work, the band energy $\varepsilon_i(\vec{k})$ was calculated by density functional theory. The group velocity of electron and hole carriers can be obtained from the gradient of the band energy $\varepsilon_i(\vec{k})$ in $\vec{k}$-space, $v(i,\vec{k}) = \nabla\varepsilon_i(\vec{k})/\hbar$. In our band energy calculations, the $\vec{k}$-mesh is chosen as $64 \times 64 \times 1$ for the two-dimensional sheet, which is fine enough to give converged relaxation time and mobility. The relaxation time $\tau_\alpha(i,\vec{k})$ is calculated by the collision term in the Boltzmann method,[44] and within the deformation potential formalism, it can be written as

$$\frac{1}{\tau_\alpha(i,\vec{k})} = k_B T \frac{2\pi E_1^2}{\hbar C^\beta} \sum_{k'\in BZ} \left\{ \left[1 - \frac{\vec{v}_\alpha(\vec{k}')}{\vec{v}_\alpha(\vec{k})}\right] \delta[\varepsilon(\vec{k}') - \varepsilon(\vec{k})] \right\} \quad (3)$$

Here the delta function denotes that the scattering process is elastic and occurs between the band states with the same band index. E_1 is the DP constant of the i-th band, and C^β is the elastic constant along the direction β. In principle, different scattering channels can be added in the following way:

$$\frac{1}{\tau} = \frac{1}{\tau_{ac}} + \frac{1}{\tau_{op}} + \frac{1}{\tau_{imp}} + \quad \ldots \quad (4)$$

where ac, op, and imp denote acoustic, optical phonons, and impurity respectively. Here, we only consider the acoustic phonon scattering.

Acknowledgment. This work is supported by the National Natural Science Foundation of China and the Ministry of Science and Technology of China.

Supporting Information Available: Γ-point degenerate HOMO and LUMO and corresponding energies before and after dilation. This material is available free of charge via the Internet at http://pubs.acs.org.

REFERENCES AND NOTES

1. Kroto, H. W.; Heath, J. R.; Obrien, S. C.; Curl, R. F.; Smalley, R. E. C60: Buckminsterfullerene. *Nature* **1985,** *318*, 162–163.
2. Iijima, S. Helical Microtubules of Graphitic Carbon. *Nature* **1991,** *354*, 56–58.
3. Novoselov, K. S.; Geim, A. K.; Morozov, S. V.; Jiang, D.; Zhang, Y.; Dubonos, S. V.; Grigorieva, I. V.; Firsov, A. A. Electric Field Effect in Atomically Thin Carbon Films. *Science* **2004,** *306*, 666.
4. Baughman, R. H.; Eckhardt, H.; Kertesz, M. Structure Property Predictions for New Planar Forms of Carbon-Layered Phases Containing sp2 and sp Atoms. *J. Chem. Phys.* **1987,** *87*, 6687–6699.
5. Haley, M. M.; Brand, S. C.; Pak, J. J. Carbon Networks Based on Dehydrobenzoannulenes: Synthesis of Graphdiyne Substructures. *Angew. Chem., Int. Ed.* **1997,** *36*, 836.
6. Haley, M. M.; Bell, M. L.; English, J. J.; Johnson, C. A.; Weakley, T. J. R. Versatile Synthetic Route to and DSC Analysis of Dehydrobenzoannulenes: Crystal Structure of a Heretofore Inaccessible 20 Annulene Derivative. *J. Am. Chem. Soc.* **1997,** *119*, 2956–2957.

7. Wan, W. B.; Haley, M. M. Carbon Networks Based on Dehydrobenzoannulenes. 4. Synthesis of "Star" and "Trefoil" Graphdiyne Substructures *via* Sixfold Cross-Coupling of Hexaiodobenzene. *J. Org. Chem.* **2001,** *66*, 3893–3901.
8. Marsden, J. A.; Haley, M. M. Carbon Networks Based on Dehydrobenzoannulenes. 5. Extension of Two-Dimensional Conjugation in Graphdiyne Nanoarchitectures. *J. Org. Chem.* **2005,** *70*, 10213.
9. Li, G. X.; Li, Y. L.; Liu, H. B.; Guo, Y. B.; Li, Y. J.; Zhu, D. B. Architecture of Graphdiyne Nanoscale Films. *Chem. Commun.* **2010,** *46*, 3256–3258.
10. Haley, M. M.; Wan, W. B. Natural and Non-natural Planar Carbon Networks: From Monomeric Models to Oligomeric Substructures. *Adv. Strained Interesting Org. Mol.* **2000,** *8*, 1–41.
11. Balaban, A. T.; Rentia, C. C.; Ciupitu, E. Chemical Graphs. 6. Estimation of Relative Stability of Several Planar and Tridimensional Lattices for Elementary Carbon. *Rev. Roum. Chim.* **1968,** *13*, 231–247.
12. Narita, N.; Nagai, S.; Suzuki, S.; Nakao, K. Optimized Geometries and Electronic Structures of Graphyne and Its Family. *Phys. Rev. B* **1998,** *58*, 11009–11014.
13. Narita, N.; Nagai, S.; Suzuki, S.; Nakao, K. Electronic Structure of Three-Dimensional Graphyne. *Phys. Rev. B* **2000,** *62*, 11146–11151.
14. Narita, N.; Nagai, S.; Suzuki, S. Potassium Intercalated Graphyne. *Phys. Rev. B* **2001,** *64*, 245408.
15. Kondo, M.; Nozaki, D.; Tachibana, M.; Yumura, T.; Yoshizawa, K. Electronic Structures and Band Gaps of Chains and Sheets Based on Phenylacetylene Units. *Chem. Phys.* **2005,** *312*, 289–297.
16. Diederich, F.; Rubin, Y. Synthetic Approaches Toward Molecular and Polymeric Carbon Allotropes. *Angew. Chem., Int. Ed. Engl.* **1992,** *31*, 1101–1123.
17. Diederich, F. Carbon Scaffolding: Building Acetylenic All-Carbon and Carbon-Rich Compounds. *Nature* **1994,** *369*, 199–207.
18. Bunz, U. H. F.; Rubin, Y.; Tobe, Y. Polyethynylated Cyclic Pi-systems: Scaffoldings for Novel Two and Three-dimensional Carbon Networks. *Chem. Soc. Rev.* **1999,** *28*, 107–119.
19. Wan, W. B.; Brand, S. C.; Pak, J. J.; Haley, M. M. Synthesis of Expanded Graphdiyne Substructures. *Chem.—Eur. J.* **2000,** *6*, 2044.
20. Baughman, R. H.; Zakhidov, A. A.; de Heer, W. A. Carbon Nanotubes—The Route toward Applications. *Science* **2002,** *297*, 787–792.
21. Avouris, P.; Chen, Z. H.; Perebeinos, V. Carbon-Based Electronics. *Nat. Nanotechnol.* **2007,** *2*, 605–615.
22. Lin, Y. M.; Jenkins, K. A.; Valdes-Garcia, A.; Small, J. P.; Farmer, D. B.; Avouris, P. Operation of Graphene Transistors at Gigahertz Frequencies. *Nano Lett.* **2009,** *9*, 422–426.
23. Durkop, T.; Getty, S. A.; Cobas, E.; Fuhrer, M. S. Extraordinary Mobility in Semiconducting Carbon Nanotubes. *Nano Lett.* **2004,** *4*, 35–39.
24. Berger, C.; Song, Z. M.; Li, X. B.; Wu, X. S.; Brown, N.; Naud, C.; Mayou, D.; Li, T. B.; Hass, J.; Marchenkov, A. N.; *et al.* Electronic Confinement and Coherence in Patterned Epitaxial Graphene. *Science* **2006,** *312*, 1191–1196.
25. Tan, Y. W.; Zhang, Y.; Bolotin, K.; Zhao, Y.; Adam, S.; Hwang, E. H.; Das Sarma, S.; Stormer, H. L.; Kim, P. Measurement of Scattering Rate and Minimum Conductivity in Graphene. *Phys. Rev. Lett.* **2007,** *99*, 246803.
26. Bolotin, K. I.; Sikes, K. J.; Jiang, Z.; Klima, M.; Fudenberg, G.; Hone, J.; Kim, P.; Stormer, H. L. Ultrahigh Electron Mobility in Suspended Graphene. *Solid State Commun.* **2008,** *146*, 351–355.
27. Chen, J. H.; Jang, C.; Xiao, S. D.; Ishigami, M.; Fuhrer, M. S. Intrinsic and Extrinsic Performance Limits of Graphene Devices on SiO_2. *Nat. Nanotechnol.* **2008,** *3*, 206–209.
28. Du, X.; Skachko, I.; Barker, A.; Andrei, E. Y. Approaching Ballistic Transport in Suspended Graphene. *Nat. Nanotechnol.* **2008,** *3*, 491–495.
29. Orlita, M.; Faugeras, C.; Plochocka, P.; Neugebauer, P.; Martinez, G.; Maude, D. K.; Barra, A. L.; Sprinkle, M.; Berger, C.; de Heer, W. A.; *et al.* Approaching the Dirac Point in High-Mobility Multilayer Epitaxial Graphene. *Phys. Rev. Lett.* **2008,** *101*, 267601.
30. Chen, F.; Xia, J. L.; Ferry, D. K.; Tao, N. J. Dielectric Screening Enhanced Performance in Graphene FET. *Nano Lett.* **2009,** *9*, 2571–2574.
31. Bardeen, J.; Shockley, W. Deformation Potentials and Mobilities in Non-polar Crystals. *Phys. Rev.* **1950,** *80*, 72–80.
32. Long, M. Q.; Tang, L.; Wang, D.; Wang, L. J.; Shuai, Z. G. Theoretical Predictions of Size-Dependent Carrier Mobility and Polarity in Graphene. *J. Am. Chem. Soc.* **2009,** *131*, 17728–17729.
33. Neugebauer, P.; Orlita, M.; Faugeras, C.; Barra, A. L.; Potemski, M. How Perfect Can Graphene Be?. *Phys. Rev. Lett.* **2009,** *103*, 136403.
34. Beleznay, F. B.; Bogar, F.; Ladik, J. Charge Carrier Mobility in Quasi-One-Dimensional Systems: Application to a Guanine Stack. *J. Chem. Phys.* **2003,** *119*, 5690–5695.
35. Sa, N.; Wang, G.; Yin, B.; Huang, Y. H. Theoretical Study on Non-covalent Functionalization of Armchair Carbon Nanotube by Tetrathiafulvalene Molecule. *Phys. E* **2008,** *40*, 2396–2399.
36. Kresse, G.; Hafner, J. *Ab Initio* Molecular Dynamics for Liquid Metals. *Phys. Rev. B* **1993,** *47*, 558–561.
37. Kresse, G.; Hafner, J. *Ab Initio* Molecular-Dynamics Simulation of the Liquid-Metal-Amorphous-Semiconductor Transition in Germanium. *Phys. Rev. B* **1994,** *49*, 14251–14269.
38. Kresse, G.; Furthmuller, J. Efficiency of Ab-Initio Total Energy Calculations for Metals and Semiconductors Using a Plane-Wave Basis Set. *Comput. Mater. Sci.* **1996,** *6*, 15–50.
39. Kresse, G.; Furthmuller, J. Efficient Iterative Schemes for Ab Initio Total-energy Calculations Using a Plane-Wave Basis Set. *Phys. Rev. B* **1996,** *54*, 11169–11186.
40. Kresse, G.; Joubert, D. From Ultrasoft Pseudopotentials to the Projector Augmented-Wave Method. *Phys. Rev. B* **1999,** *59*, 1758–1775.
41. Perdew, J. P.; Burke, K.; Ernzerhof, M. Generalized Gradient Approximation Made Simple. *Phys. Rev. Lett.* **1996,** *77*, 3865–3868.
42. Cheng, Y. C.; Silbey, R. J.; da Silva, D. A.; Calbert, J. P.; Cornil, J.; Bredas, J. L. Three-Dimensional Band Structure and Bandlike Mobility in Oligoacene Single Crystals: A Theoretical Investigation. *J. Chem. Phys.* **2003,** *118*, 3764–3774.
43. Tang, L.; Long, M. Q.; Wang, D.; Shuai, Z. G. The Role of Acoustic Phonon Scattering in Charge Transport in Organic Semiconductors: a First-principles Deformation-potential Study. *Sci. China, Ser. B: Chem.* **2009,** *52*, 1646–1652.
44. Ziman, J. M. *Principles of the Theory of Solids*, 2nd ed; Cambridge University Press: London, 1972; pp 211−229.